HHS Public Access

Author manuscript

J Magn Reson Imaging. Author manuscript; available in PMC 2016 January 16.

Published in final edited form as:

J Magn Reson Imaging. 2016 January ; 43(1): 181–189. doi:10.1002/jmri.24978.

Improving Thermal Dose Accuracy in Magnetic Resonance-Guided Focused Ultrasound Surgery: Long-Term Thermometry Using a Prior Baseline as a Reference

Rachel R. Bitton, PhD[1,*], **Taylor D. Webb, MS**[2], **Kim Butts Pauly, PhD**[1], and **Pejman Ghanouni, MD, PhD**[1]

[1]School of Medicine, Department of Radiology, Stanford University, Stanford, California, USA

[2]Department of Electrical Engineering, Stanford University, Stanford, California, USA

Abstract

Purpose—To investigate thermal dose volume (TDV) and non-perfused volume (NPV) of magnetic resonance-guided focused ultrasound (MRgFUS) treatments in patients with soft tissue tumors, and describe a method for MR thermal dosimetry using a baseline reference.

Materials and Methods—Agreement between TDV and immediate post treatment NPV was evaluated from MRgFUS treatments of five patients with biopsy-proven desmoid tumors. Thermometry data (gradient echo, 3T) were analyzed over the entire course of the treatments to discern temperature errors in the standard approach. The technique searches previously acquired baseline images for a match using 2D normalized cross-correlation and a weighted mean of phase difference images. Thermal dose maps and TDVs were recalculated using the matched baseline and compared to NPV.

Results—TDV and NPV showed between 47%–91% disagreement, using the standard immediate baseline method for calculating TDV. Long-term thermometry showed a nonlinear local temperature accrual, where peak additional temperature varied between 4–13°C (mean = 7.8°C) across patients. The prior baseline method could be implemented by finding a previously acquired matching baseline 61% ± 8% (mean ± SD) of the time. We found 7%–42% of the disagreement between TDV and NPV was due to errors in thermometry caused by heat accrual. For all patients, the prior baseline method increased the estimated treatment volume and reduced the discrepancies between TDV and NPV ($P = 0.023$).

Conclusion—This study presents a mismatch between in-treatment and post treatment efficacy measures. The prior baseline approach accounts for local heating and improves the accuracy of thermal dose-predicted volume.

Magnetic resonance-guided focused ultrasound (MRgFUS) has been used in clinical trials to ablate soft tissue tumors such as breast tumors, uterine fibroids, and prostate tumors. Some of these trials aimed to show safety and feasibility through partial tumor ablation.[1–5] More recently, patient studies have targeted total tumor volume ablation, including large uterine

[*]Address reprint requests to: R.R.B., Stanford University, Department of Radiology, Richard M. Lucas Center for Imaging, Mail Code 5488, Route 8, Stanford, CA 94305-5488. rbitton@stanford.edu.

fibroid volumes (>~75 cc).[6,7] For malignant tumors, ablation of the entire tumor is a necessity if MRgFUS is to be considered as an alternative to surgery; while even for benign tumors, such as uterine fibroids, achieving total ablation results in more durable symptomatic relief.[8]

Total tumor ablation demands a highly accurate method to assess treatment efficacy. MR thermometry-derived thermal dose mapping is the primary method used to assess tumor ablation during an MRgFUS procedure.[9] MR-derived proton resonance frequency shift (PRF) thermometry provides a change in temperature, which is then used to calculate thermal dose; neither absolute temperature nor absolute dose are calculated using these methods.[10] Because these are not absolute measurements, the standard method does not account for local accumulation of heat over the course of a treatment, which can cause errors in thermometry, and thus, errors in the estimated thermal dose delivered to tissue (Fig. 1).[11,12] Underestimation of thermometry and thermal dose may result in unnecessary additional sonications of tissue that has already been ablated through sonication of adjacent areas; these extra sonications provide no benefit, while increasing risks to the patient, such as skin burns. Targeting already treated tissue also prolongs the procedure time, which is a major criticism of volumetric MRgFUS compared to alternative therapies.[13–15]

Another consequence of inaccurate thermometry is the commonly reported mismatch between thermal dose treatment volume (TDV) and nonperfused volume (NPV), which is the clinically accepted standard of in vivo ablation efficacy.[7,16–19] There is potential for disagreement between the two in vivo measures (TDV, NPV) of treatment volume, as they are derived from different physical phenomena; TDV is based on temperature-dependent image-based phase accrual during treatment surpassing the threshold of 240 equivalent minutes, while NPV is based on the ability of contrast agent to reach the tissue after treatment. Because the interactions of MRI contrast and focused ultrasound ablation are not well established, contrast injections are administered only after the MRgFUS treatment is completed.[20,21] In the majority of the cases reporting mismatch, immediate posttreatment NPV exceeded thermal dose. This mismatch becomes more profound with increasing target volumes, with the error between TDV and NPV reported to be between 38%–53% for volumes >125 cc.[7] A recent preclinical treat and resect study found that the thermal dose volume underestimated ablated areas compared with both NPV and histology immediately post treatment.[22] While thermal ablation of tumor vessels, which could result in disproportionately larger NPVs, has been posited as one explanation for this discrepancy[17,23,24]; clearly, the clinical success of MRgFUS in volumetric tumor ablation depends on improving the reliability and accuracy of intraoperative treatment monitoring and assessment.

The purpose of this study was three-fold: 1) to investigate if MRgFUS desmoid treatments suffered from a mismatch between thermal dose volume and NPV; 2) to improve thermal dose mapping by accounting for accumulated heat using a prior baseline thermometry method; and 3) to assess how much of the discrepancy between TDV and NPV remained after this improvement.

Materials and Methods

General Imaging Methods

MR image data from MRgFUS treatments of five patients with biopsy-proven desmoid tumors[25] were analyzed (average age = 28 years, range 14–66 years; three men and two women). All patients were treated after providing written informed consent, and the study was approved by the local Institutional Review Board. The patients were treated under general and/or regional anesthesia using the ExAblate 2100 MR image-guided focused ultrasound system (InSightec, Tirat Carmel, Israel) on a Discovery 750w 3T magnet (General Electric, Milwaukee, WI). The target location was positioned over the transducer and the patient was strapped to the MR table to minimize motion. T_2-weighted fast spin echo images (4.9 sec repetition time, 64 msec echo time, 18–38 cm field of view, 320 × 224 matrix, 108–162 kHz bandwidth, 3–4 mm slice thickness, 39–54 slices) acquired just prior to the treatment were used for treatment planning and to calculate the starting total tumor volume. A series of spatially interleaved sonications (1.1 MHz, 20 sec, 500J–1300J) were combined to ablate a tissue volume. Each sonication was monitored using PRF thermometry. Cooling time between sonications was at least 60 seconds. The thermometry sequence uses a 2DFT spoiled gradient recalled echo (SPGR) acquired every 3.2 seconds (25 msec repetition time, 12 msec echo time, 30° flip angle, 5 mm slice thickness, 45 kHz bandwidth, 1 excitation). Contrast enhanced images were acquired immediately following the treatment using a 3D gradient echo (GRE) with fat suppression (LAVA, GE, 5.4 msec repetition time, 1.7 msec echo time, 15° flip angle, 288–320×224 matrix, 3 excitations, 25–36 cm field of view, 167 kHz bandwidth, 2–4 mm slice thickness, 56–120 slices,).

MR Thermometry and Thermal Dose Methods

PRF thermometry uses a reference phase image with no ultrasound applied that is considered a body temperature baseline image from which subsequent heating phase images are subtracted. Using complex phase subtraction, the change in temperature is calculated from the following relationship:

$$\Delta T = \frac{\phi - \phi_{baseline}}{\alpha \gamma B_0 TE} \quad (1)$$

where φ is the phase of the current image, and $\varphi_{baseline}$ is the phase of the reference image, B_0 is the magnetic field strength, γ is the gyromagnetic ratio, α is the temperature coefficient (-9.09×10^{-3} ppm/°C),[26] and TE is the echo time. Temperature maps are converted into thermal dose maps using the following equation:

$$CEM_{43} = \sum_{t=0}^{t=final} R^{(43-T)} \Delta t R = \begin{cases} 0.50, T \geq 43^{\circ}\mathrm{C} \\ 0.25, T < 43^{\circ}\mathrm{C} \end{cases} \quad (2)$$

where CEM_{43} is thermal dose in equivalent minutes at 43°C, R is a constant related to the number of minutes needed to compensate for a 1°C temperature change around the breakpoint, and T is the temperature (°C) during time Δt.[27]

Standard MR Thermometry Using the Immediate Baseline Method and Thermal Dose Calculation

During an MRgFUS treatment, the reference phase image ($\varphi_{baseline}$) is acquired just prior to the start of sonication and considered a body temperature baseline image. The ultrasound is turned on, and phase images (φ) continue to be acquired during and just after the sonication. The standard MR thermometry method described above, referred to as the "immediate baseline" method in this study, is the method implemented in the only FDA-approved and most widely used MRgFUS device. Figure 1a depicts this standard, immediate baseline method, where a new baseline is acquired for each sonication, immediately prior to the application of ultrasound at time t_{a0}. The subsequent heating images are acquired at timepoints t_{a1}, t_{a2}.… All images were reconstructed both with this method and with the prior baseline method described below. To assess the contribution of phase drift accumulation,[28] a background tissue region outside the heating path was examined over the course of the treatment. Changes in later baseline phase images were compared to prior baseline phase images acquired at that location.

Analysis of Thermometry Baseline Errors

Figure 1b illustrates a problem where accumulation of heat shifts the actual temperature curve; this means that the assumption that the starting reference temperature for the tissue prior to sonication is 37°C (body temperature) is incorrect. To determine if this type of heat accumulation was occurring, baselines throughout the course of the treatment that shared the same slice location were compared with each other. The earliest acquired baseline prior to ultrasound was used as the reference, and later sonication baselines (prior to ultrasound) were converted into temperature maps using complex phase subtraction.

Prior Baseline MR Thermometry and Thermal Dose Calculation

The prior baseline approach aims to calculate temperature using a baseline, or reference image acquired early in a treatment, when the assumption that the reference image is at body temperature is valid. The algorithm searches previously acquired sonication baseline images for a match in the slice location. The matched image is used as the reference to calculate temperature maps for subsequent sonications. Figure 2 shows the basic algorithm structure. The algorithm criteria for a prior baseline similarity match include: 1) 2D normalized cross-correlation of magnitude images to check for motion, and 2) magnitude weighted mean of the phase difference images between prior and immediate baselines to check for large phase difference errors. If no appropriate prior baseline is found, the immediate baseline image is used. The peak of the 2D normalized cross-correlation, r_m, is considered the similarity value between the prior baseline magnitude image, and a baseline magnitude image acquired later in the treatment. Inclusion of the prior baseline was done for r_m values >0.80 because magnitude images that were at least 80% similar were considered to not have significant disagreement due to motion.

If the baseline image met the magnitude match criteria, the image was checked for large phase variations. First, subtracted phase images were weighted by the normalized magnitude image to mask random phase noise outside the image area, given by the following:

$$W(x,y)=\left|\tan^{-1}\left(\frac{\phi(x,y)}{\phi_{\text{baseline}}(x,y)}\right)\right|\cdot m_b(x,y) \Big/ \sum_{x=0}^{n}\sum_{y=0}^{n} m_b(x,y) \quad (3)$$

where $W(x,y)$ is the weighted image and $m_b(x,y)$ is the baseline normalized magnitude image. The maximum phase/temperature variation, T_v, of the weighted phase image, $W(x,y)$, was restricted to $T_v \leq 25\%$ of the mean phase value, given by $T_v = W(x,y)/\bar{W}$. The thermal dose is calculated by the same relationship as immediate baseline (Eq. (2)), where T is now the temperature using prior baseline thermometry.

The prior baseline method performance was evaluated by determining 1) how often a previously acquired baseline existed; 2) how often a prior baseline met the matching criteria; and 3) what was the earliest baseline that was used.

TDV and NPV Comparison

Thermal dose ablation volumes and non perfused ablation volumes were examined to compare agreement between the two measures. The treatment volumes were derived from MR thermometry and from immediate post treatment contrast enhanced imaging. TDVs were calculated as the area of pixels whose dose value met or exceeded the thermal lethal dose threshold of 240_{CEM} ($\text{CEM}_{43} = 240$) multiplied by the slice thickness, for each slice in the volume. TDVs were calculated both for the immediate baseline MR thermometry method and the prior baseline method. NPVs were defined as the non perfused area in each slice multiplied by the slice thickness, measured from post treatment CE images. A radiologist (P.G., with 4 years of experience in MR image interpretation) drew the contours of the non enhancing portion of the tumor on each slice of the treated volume.

Results

A representative cumulative thermal dose map overlaid on the magnitude image for a given slice location is shown in Fig. 3a for two patients. Figure 3b shows the corresponding post treatment contrast-enhanced image. The non perfused contour is larger than the lethal dose contour of the thermal dose map for both patients.

The results of the comparison between all five patients are shown in Table 1. The measured treatment volumes report 47%–91% disagreement between TDV and NPV.

The analysis of baselines for a given slice location throughout a treatment reveals errors in the assumption made during standard MR thermometry that the temperature returns to baseline (37°C) between sonications (Fig. 4). If the body temperature assumption was correct, no temperature rise would be present between baselines. However, as seen in this representative treatment, as the treatment progressed from sonication #64 to sonication #74 (a 32 minute interval) a local temperature rise of up to 13°C in the region of treatment is visible, indicating insufficient cooling between sonications. With such a temperature rise, the tissue can receive lethal dose in under 2 minutes; if this temperature accumulation were prospectively monitored, this would allow for decreased treatment time. Peak additional temperature varied between 4–13°C (mean = 7.8°C) across patients. A region of tissue far

from the treated area shows the consistency of the background phase. This indicates that the phase drift effects over the course of the treatment were not significant, as the background is within the ±1°C error of the temperature measurements.

The TDV calculation with both the standard immediate baseline calculation (blue curve) and the prior baseline calculation (green curve) over the course of the entire treatment is shown in Fig. 5. The error is the difference between these two curves, which is seen to increase as the treatment progresses. This demonstrates why these errors are more prevalent in large treatment volumes.[7]

The prior baseline technique was applied to each patient case and treatment volumes were recalculated. Prior baselines could only be applied in cases where a sonication occurred at a specific slice location more than once, and the prior baseline was not corrupted by patient motion or significant phase variation due to transducer susceptibility (Table 2). The technique allowed 61% ± 8% (mean ± SD) of the sonications to be recalculated using a previously acquired baseline. A single slice location could be visited more than once, with sonications varying spatially within the slice. For this reason, many sonications had more than one prior baseline to search from. In those cases, the algorithm picked the earliest possible matching baseline. The mean baseline shows a treatment average of how early a reference baseline was used, where 1 is the first baseline acquired at that location, 2 is the second acquired, and so on. The treatment with the least impact from the technique was partly corrupted by patient motion, which occurred after 3 hours of time on the MRI table (patient 5). This resulted in the fewest prior baseline matches (48%) overall, and those that did match were acquired later in the treatment (mean baseline = 2.23), when heat accumulation had already occurred. With the exception of patient 5, the prior baseline method showed the majority of dose recalculations were able to utilize the first possible baseline (mean baseline = 1.17– 1.33), for patients 1–4.

In Fig. 6, example dose overlays and post treatment image comparisons are provided for three patients. The images show a comparison of dose contours between the methods. In all cases, the dose area increases with application of the prior baseline technique compared to the standard immediate baseline method. A small amount of noise in thermal dose is visible in low signal areas of the thermometry images, and contributes to the overall computed thermal dose volume. The prior baseline contour approaches the NPV contour, while not achieving complete contour agreement.

A comparison of the treatment volumes predicted using the immediate baseline and prior baseline methods are shown in Fig. 7. The volumes are given as a ratio of the NPV for each patient. A ratio of 1 indicates complete agreement between TDV and NPV. For each patient, the application of the prior baseline method increased the estimated treatment volume and improved the agreement ($P = 0.023$ using a paired two tailed *t*-test).

Discussion

The results from this study showed disagreements between the two accepted measures of treatment efficacy: thermal dose volume and NPV, the accepted gold standard. Compared to

NPVs, thermal dose volumes underestimated the treatment areas, resulting in unnecessary sonications that extended treatment times. Our findings revealed that between 7%–42% of the disagreement was due to errors in thermometry caused by the incorrect assumption that there is complete return to baseline body temperature (37°C) between sonications. Temperature maps of baselines showed local heat accumulation in the region of treatment due to insufficient cooling between sonications. By applying the prior baseline technique to account for this heat accumulation, sonication times could potentially be shortened and unnecessary sonications could even be eliminated. Note that heat accumulation occurred in these procedures despite increasing the required cooling time of 60–70 seconds, set by the system, to an average of 100–140 seconds (this increased cooling time was used in these treatments for planning between sonications). An additional increase in cooling times would be a clinically prohibitive solution since this would further prolong already long treatments; instead, the prior baseline method was applied to account for accumulated heat. The results show that thermal dose area increased for each case where prior baselines could be applied. We have shown that the prior baseline method reduced the discrepancy between thermal dose volume and NPV, although still predicting smaller treatment volumes than post treatment imaging reports for all patients in this study. The most practical implementation of the prior baseline would be to periodically acquire a volume of no-ultrasound reference images to use as a library throughout the treatment. This library could be acquired during cooling periods between sonications, minimizing any impact on the treatment time. Although this proposed method to improve TDV measurements may not eliminate all discrepancies with NPV, it would be an important first step that would reduce the discrepancy, and a necessary step prior to invoking and exploring additional more complicated and more difficult to prove causes of mismatch between TDV and NPV.

The target treatment volume plays a large role in the effect of heat accumulation. Larger ablation volumes require an increased number of sonications, potentially resulting in heat accumulation in tissues along the beam path. In the case of patient 2, with a large tumor volume of 104 cc, intervening healthy muscle tissue in the near field was also ablated. The findings of this study suggest that the thermometry errors resulting from insufficient cooling are more profound as the target volume (and hence treatment time) increases, and dose volume may exhibit a nonlinear response through the course of the treatment. The physiological reasons behind this heat accumulation may be due to the complete ablation of tissue in, and adjacent to, the target region. Perfusion and subsequent cooling of ablated tissue is reduced, resulting in local heat accumulation. Patient-dependent factors that also play a role in locally increased heat due to inherent acoustic properties of tissue include: highly absorbing bone in the far field,[29,30] nonvascular or fibrous tumor tissue types, intervening tissue with increased energy absorption,[31,32] as in muscle or fascia, and intervening tissue with heat insulation properties, as in adipose tissue.[33]

The TDV-NPV mismatch reported here is not unique to desmoid tumors, as our findings are in agreement with recent studies in fibroid tumors showing underestimation of thermal dose volume.[7,17,19] The high vascularity of some fibroid tumors may confound the relationship between thermal dose volume and NPV. For example, vessel occlusion due to ablation can result in ischemic areas, contributing to NPV[17,23,24]; however, we observed similar findings even though desmoids are less vascular tumors.

A limitation to the prior baseline method as it is presented in this study is that the algorithm relies on similar imaging planes for different sonication locations. In order for the algorithm to be applied retrospectively to treatments without repeated imaging planes (ex: oblique planes centered at the focus), the thermal dose images could be mapped in 3D space. Another limitation in this type of long time scale approach to thermometry is corruption by patient motion; for example, respiratory motion could corrupt MR thermometry when treating the upper abdomen. As mentioned above, the periodic acquisition of a library of baselines not only through a treatment volume, but also throughout a complete respiratory cycle may account for respiratory motion, and has been shown in MRgFUS in the liver.[34] In addition, robust rotational and out-of-plane motion correction algorithms are still under investigation and can be computationally expensive.[35,36] Note that improved thermometry and shorter procedure times also have the potential to reduce patient motion. Another limitation of this approach is its reliance on standard 2D temperature imaging, with dose calculated from a single slice centered at the focus. When multislice temperature acquisition is used, a small portion of the dose, estimated at up to 5%, may be seen on slices around the central slice. This also contributes to the mismatch between TDV and NPV. Volumetric thermometry would reduce this discrepancy, but at the expense of lower temporal resolution, which would also then impact the ability to rapidly detect tissue cavitation. Finally, this study is limited by the small number of patients and by the application of the technique to a single tumor type. The method described here is currently being assessed with a larger patient population and in multiple tumor types.

A number of other approaches could contribute to improve the accuracy of thermometry and dosimetry. When ablation temperatures are high, dose can continue to accumulate after the ultrasound has been turned off. This is due to the equivalent minute relationship given in Eq. (2). The current protocol acquires only two post sonication phases to confirm cooling is occurring. However, continuous imaging during the cooling periods between sonications would capture some of this additional dose directly, while extrapolation techniques could further improve the dose accuracy. Additionally, the 240CEM_{43} criteria is a derived equation for thermal dose that relies on measured constants that can vary between tissue types and can be affected by thermal intolerance phenomena.[27,37,38] Some research has found better agreement between NPV and TDV with a lower CEM lethal dose threshold; however, additional studies are required to validate their use for various tissue types in vivo.[17,39] Further investigation into the derivation of thermal dose could be helpful, as well as development of absolute MR thermometry.[40–43]

Underestimation of thermal dose due to thermometry errors has significant clinical impact. A better in-treatment efficacy measure such as improved thermal dosimetry using the prior baseline method has the potential to increase safety. First, the energy required to achieve ablation can be reduced when the reference temperature is already elevated. Second, by accounting for accumulated heat, and hence accumulated dose, the prior baseline method may allow elimination of unnecessary sonications in areas already ablated through cumulative heating. Decreasing the energy or number of sonications leads to less heat accumulation on the skin and other healthy structures, limiting the risk of damage to healthy intervening tissues. For example, the unintended ablation of gluteal muscle reported for patient 2 might have been avoided if knowledge of the nonlinear heat accumulation in that

region was known. More accurate thermometry resulting in fewer sonications would also reduce treatment times, which has been a major criticism of MRgFUS for volumetric ablation. Treatment time reduction would also be cost-effective and less demanding on the patient. For the prior baseline method to improve safety and reduce treatment times, it must be applied during the treatment, rather than retrospectively. This currently requires the ability to pull thermometry images to a separate workstation for real-time postprocessing, which must occur rapidly enough to inform the treating physician prior to the next sonication. Such postprocessing tools are now in use at our institution. Alternatively, the vendors could integrate these tools in subsequent versions of their software.

In conclusion, the results of this study present a problem of mismatch between in-treatment and post treatment measures of successful ablation in the use of MRgFUS, and show that a prior baseline long-term thermometry approach can improve accuracy of thermal dose predicted volume. This technique would improve safety and allow the treatment to end sooner, improving clinical feasibility of noninvasive MRgFUS in volumetric tumor ablations.

Acknowledgments

Authors would like to thank Shannon Walters and Joseph Munaretto for helpful discussions in non perfused volume ROIs and algorithm development (respectively). Contract grant sponsor: Magnetic Resonance Imaging-Guided Cancer Interventions, KB Pauly (PI); Contract grant number: NIH P01 CA159992.

References

1. Napoli A, Anzidei M, De Nunzio C, et al. Real-time magnetic resonance-guided high-intensity focused ultrasound focal therapy for localised prostate cancer: preliminary experience. Eur Urol. 2013; 63:395–398. [PubMed: 23159454]
2. Leslie T, Ritchie R, Illing R, et al. High-intensity focused ultrasound treatment of liver tumours: post-treatment MRI correlates well with intra-operative estimates of treatment volume. Br J Radiol. 2012; 85:1363–1370. [PubMed: 22700259]
3. Zhang L, Chen W-Z, Liu Y-J, et al. Feasibility of magnetic resonance imaging-guided high intensity focused ultrasound therapy for ablating uterine fibroids in patients with bowel lies anterior to uterus. Eur J Radiol. 2010; 73:396–403. [PubMed: 19108974]
4. Furusawa H, Namba K, Thomsen S, et al. Magnetic resonance-guided focused ultrasound surgery of breast cancer: reliability and effectiveness. J Am Coll Surg. 2006; 203:54–63. [PubMed: 16798487]
5. LeBlang SD, Hoctor K, Steinberg FL. Leiomyoma shrinkage after MRI-guided focused ultrasound treatment: report of 80 patients. Am J Roentgenol. 2010; 194:274–280. [PubMed: 20028933]
6. Trumm CG, Stahl R, Clevert D-A, et al. Magnetic resonance imaging-guided focused ultrasound treatment of symptomatic uterine fibroids: impact of technology advancement on ablation volumes in 115 patients. Invest Radiol. 2013; 48:359–365. [PubMed: 23385396]
7. Voogt MJ, Trillaud H, Kim YS, et al. Volumetric feedback ablation of uterine fibroids using magnetic resonance-guided high intensity focused ultrasound therapy. Eur Radiol. 2012; 22:411–417. [PubMed: 21901565]
8. Mindjuk I, Trumm CG, Herzog P, Stahl R, Matzko M. MRI predictors of clinical success in MR-guided focused ultrasound (MRgFUS) treatments of uterine fibroids: results from a single centre. Eur Radiol. 2015; 26:1317–1328. [PubMed: 25510445]
9. Hynynen K. MRI-guided focused ultrasound treatments. Ultrasonics. 2010; 50:221–229. [PubMed: 19818981]
10. Kim YS, Trillaud H, Rhim H, Lim HK, Mali W, Voogt M, et al. MR thermometry analysis of sonication accuracy and safety margin of volumetric MR imaging-guided high-intensity focused

ultrasound ablation of symptomatic uterine fibroids. Radiology. 2012; 265:627–637. [PubMed: 23012465]

11. Vykhodtseva NI, Hynynen K, Damianou C. Pulse duration and peak intensity during focused ultrasound surgery: theoretical and experimental effects in rabbit brain in vivo. Ultrasound Med Biol. 1994; 20:987–1000. [PubMed: 7886858]
12. McDannold NJ, Jolesz FA, Hynynen KH. Determination of the optimal delay between sonications during focused ultrasound surgery in rabbits by using MR imaging to monitor thermal buildup in vivo. Radiology. 1999; 211:419–426. [PubMed: 10228523]
13. Schlesinger D, Benedict S, Diederich C, Gedroyc W, Klibanov A, Larner J. MR-guided focused ultrasound surgery, present and future. Med Phys. 2013; 40:080901. [PubMed: 23927296]
14. Tempany CMC, McDannold NJ, Hynynen K, Jolesz FA. Focused ultrasound surgery in oncology: overview and principles. Radiology. 2011; 259:39–56. [PubMed: 21436096]
15. Jolesz FA, McDannold N. Current status and future potential of MRI-guided focused ultrasound surgery. J Magn Reson Imaging. 2008; 27:391–399. [PubMed: 18219674]
16. Rabinovici J, Inbar Y, Revel A, et al. Clinical improvement and shrinkage of uterine fibroids after thermal ablation by magnetic resonance-guided focused ultrasound surgery. Ultrasound Obstet Gynecol. 2007; 30:771–777. [PubMed: 17899577]
17. McDannold N, Tempany CM, Fennessy FM, et al. Uterine leiomyomas: MR imaging-based thermometry and thermal dosimetry during focused ultrasound thermal ablation. Radiology. 2006; 240:263–272. [PubMed: 16793983]
18. Hindley J, Gedroyc WM, Regan L, et al. MRI guidance of focused ultrasound therapy of uterine fibroids: early results. AJR Am J Roentgenol. 2004; 183:1713–1719. [PubMed: 15547216]
19. Machtinger R, Inbar Y, Cohen-Eylon S, Admon D, Alagem-Mizrachi A, Rabinovici J. MR-guided focus ultrasound (MRgFUS) for symptomatic uterine fibroids: predictors of treatment success. Hum Reprod. 2012; 27:3425–3431. [PubMed: 23019304]
20. Roberts A. Magnetic resonance-guided focused ultrasound for uterine fibroids. Semin Intervent Radiol. 2008; 25:394–405. [PubMed: 21326581]
21. Kim Y-S, Bae D-S, Park MJ, et al. Techniques to expand patient selection for MRI-guided high-intensity focused ultrasound ablation of uterine fibroids. Am J Roentgenol. 2014; 202:443–451. [PubMed: 24450690]
22. Wijlemans JW, Deckers R, van den Bosch MAAJ, et al. Evolution of the ablation region after magnetic resonance-guided high-intensity focused ultrasound ablation in a V×2 tumor model. Invest Radiol. 2013; 48:381–386. [PubMed: 23399810]
23. Pilatou MC, Stewart EA, Maier SE, et al. MRI-based thermal dosimetry and diffusion-weighted imaging of MRI-guided focused ultrasound thermal ablation of uterine fibroids. J Magn Reson Imaging. 2009; 29:404–411. [PubMed: 19161196]
24. Voogt MJ, van Stralen M, Ikink ME, et al. Targeted vessel ablation for more efficient magnetic resonance-guided high-intensity focused ultrasound ablation of uterine fibroids. Cardiovasc Intervent Radiol. 2012; 35:1205–1210. [PubMed: 22146977]
25. Walczak BE, Rose PS. Desmoid: the role of local therapy in an era of systemic options. Curr Treat Options Oncol Springer US. 2013; 14:465–473.
26. Chung AH, Jolesz FA, Hynynen K. Thermal dosimetry of a focused ultrasound beam in vivo by magnetic resonance imaging. Med Phys. 1999; 26:2017. [PubMed: 10505893]
27. Sapareto SA, Dewey WC. Thermal dose determination in cancer therapy. Int J Radiat Oncol Biol Phys. 1984; 10:787–800. [PubMed: 6547421]
28. Bandettini PA, Jesmanowicz A, Wong EC, Hyde JS. Processing strategies for time-course data sets in functional MRI of the human brain. Magn Reson Med. 1993; 30:161–173. [PubMed: 8366797]
29. Webb, T.; Bitton, R.; Ghanouni, P.; Butts Pauly, K. Spatial and Temporal Characteristics of Soft Tissue Heating in MR-HIFU. Proc 22nd Annual Meeting ISMRM; Milan. 2014. p. 2344
30. Scott SJ, Prakash P, Salgaonkar V, et al. Approaches for modelling interstitial ultrasound ablation of tumours within or adjacent to bone: theoretical and experimental evaluations. Int J Hyperthermia. 2013; 29:629–642. [PubMed: 24102393]
31. Chen L, Haar ter G, Hill CR. Influence of ablated tissue on the formation of high-intensity focused ultrasound lesions. Ultrasound Med Biol. 1997; 23:921–931. [PubMed: 9300996]

32. Damianou CA, Sanghvi NT, Fry FJ, Maass-Moreno R. Dependence of ultrasonic attenuation and absorption in dog soft tissues on temperature and thermal dose. J Acoust Soc Am. 1997; 102:628–634. [PubMed: 9228822]
33. Duck, FA. Physical properties of tissue. New York: Academic Press; 1990.
34. Holbrook AB, Ghanouni P, Santos JM, Dumoulin C, Medan Y, Pauly KB. Respiration based steering for high intensity focused ultrasound liver ablation. Magn Reson Med Wiley Online Library. 2014; 71:797–806.
35. Loktyushin A, Nickisch H, Pohmann R, Schölkopf B. Blind retrospective motion correction of MR images. Magn Reson Med. 2013; 70:1608–1618. [PubMed: 23401078]
36. Schmidt JFM, Buehrer M, Boesiger P, Kozerke S. Nonrigid retrospective respiratory motion correction in whole-heart coronary MRA. Magn Reson Med. 2011; 66:1541–1549. [PubMed: 21604297]
37. Sapareto SA. Thermal isoeffect dose: addressing the problem of thermotolerance. Int J Hyperthermia. 1987; 3:297–305. [PubMed: 3668311]
38. Dewhirst MW, Viglianti BL, Lora-Michiels M, Hanson M, Hoopes PJ. Basic principles of thermal dosimetry and thermal thresholds for tissue damage from hyperthermia. Int J Hyperthermia. 2003; 19:267–294. [PubMed: 12745972]
39. McDannold NJ, King RL, Jolesz FA, Hynynen KH. Usefulness of MR imaging-derived thermometry and dosimetry in determining the threshold for tissue damage induced by thermal surgery in rabbits. Radiology. 2000; 216:517–523. [PubMed: 10924580]
40. Kuroda K, Oshio K, Chung AH, Hynynen K, Jolesz FA. Temperature mapping using the water proton chemical shift: a chemical shift selective phase mapping method. Magn Reson Med. 1997; 38:845–851. [PubMed: 9358461]
41. Kuroda K, Mulkern RV, Oshio K, et al. Temperature mapping using the water proton chemical shift: self-referenced method with echoplanar spectroscopic imaging. Magn Reson Med. 2000; 43:220–225. [PubMed: 10680685]
42. Thrippleton MJ, Parikh J, Harris BA, et al. Reliability of MRSI brain temperature mapping at 1.5 and 3 T. NMR Biomed. 2014; 27:183–190. [PubMed: 24273188]
43. Inoue T, Shimizu H, Fujimura M, et al. Noninvasive measurement of human brain temperature adjacent to arteriovenous malformation using 3.0T magnetic resonance spectroscopy. Clin Neurol Neurosurg. 2013; 115:445–449. [PubMed: 22766254]

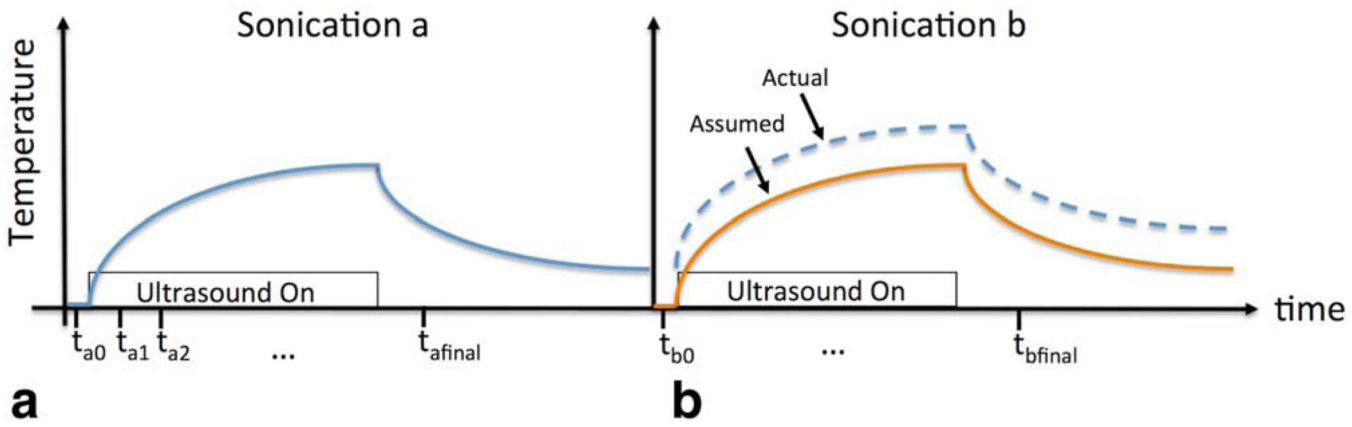

FIGURE 1.

Sonication thermometry protocol. **a:** At timepoint t_{a0} a baseline reference image prior to turning on ultrasound is acquired. Images are acquired every 3.2 seconds throughout the sonication period. The final image t_{afinal} is acquired after the ultrasound has been turned off for two 3.2-second intervals. Images are not acquired through the remainder of the cooling period. **b:** The following sonication where the assumption is made that baseline temperature has returned to 37°C. However, in cases of local heat accumulation the curve may actually be shifted due to insufficient tissue cooling between sonications.

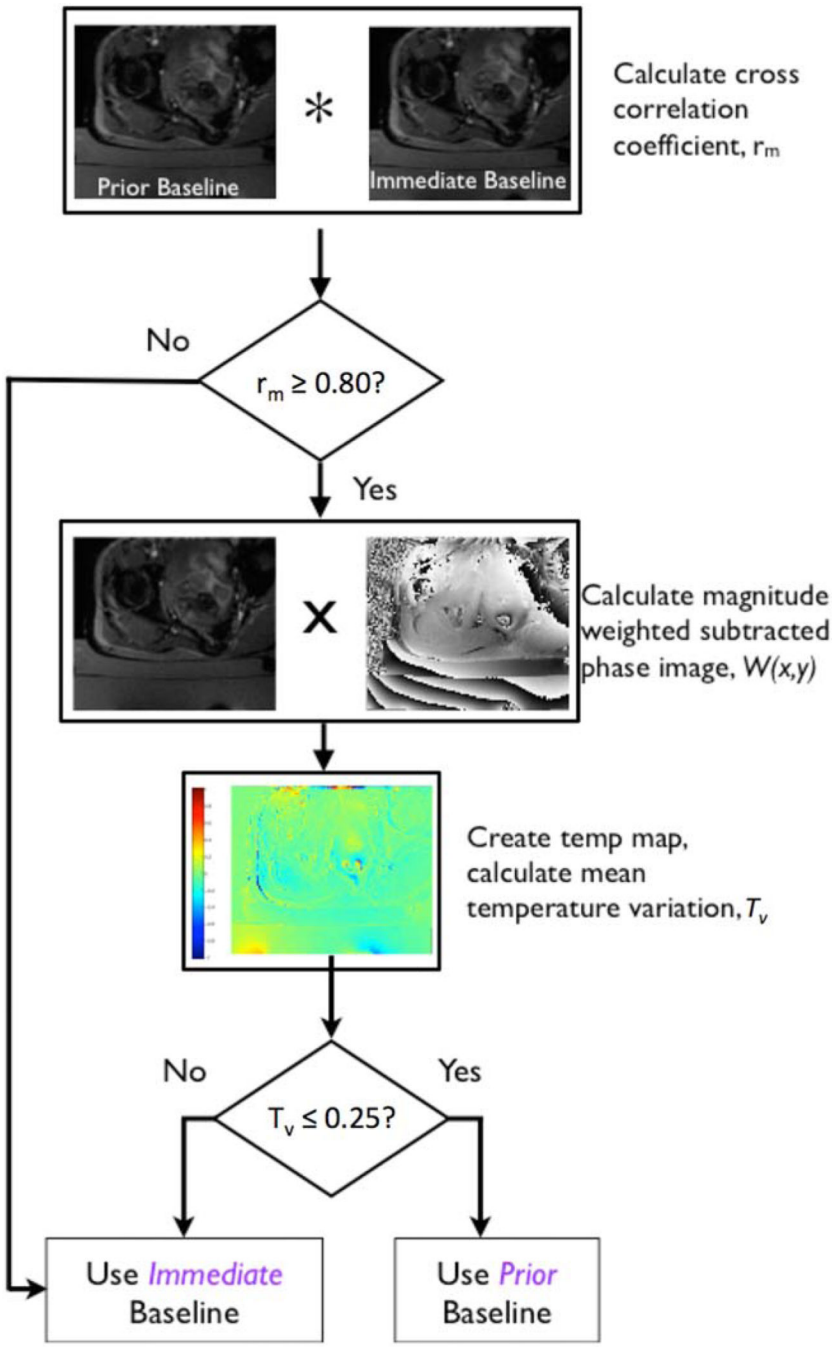

FIGURE 2.

Prior baseline algorithm flow chart. The algorithm compares the similarity of an immediate baseline with a prior baseline to determine if the prior baseline can be used to calculate thermal dose. The decision points are based on similarity of the magnitude images, and overall phase consistency. The 2D cross-correlation criteria excludes baselines where magnitude images are dissimilar due to motion. Phase subtracted images are weighted by the magnitude image to suppress low signal areas, such as background noise outside the patient.

The weighted subtracted baseline images are converted into temperature maps. The mean temperature variation criterion excludes baselines with large phase variations.

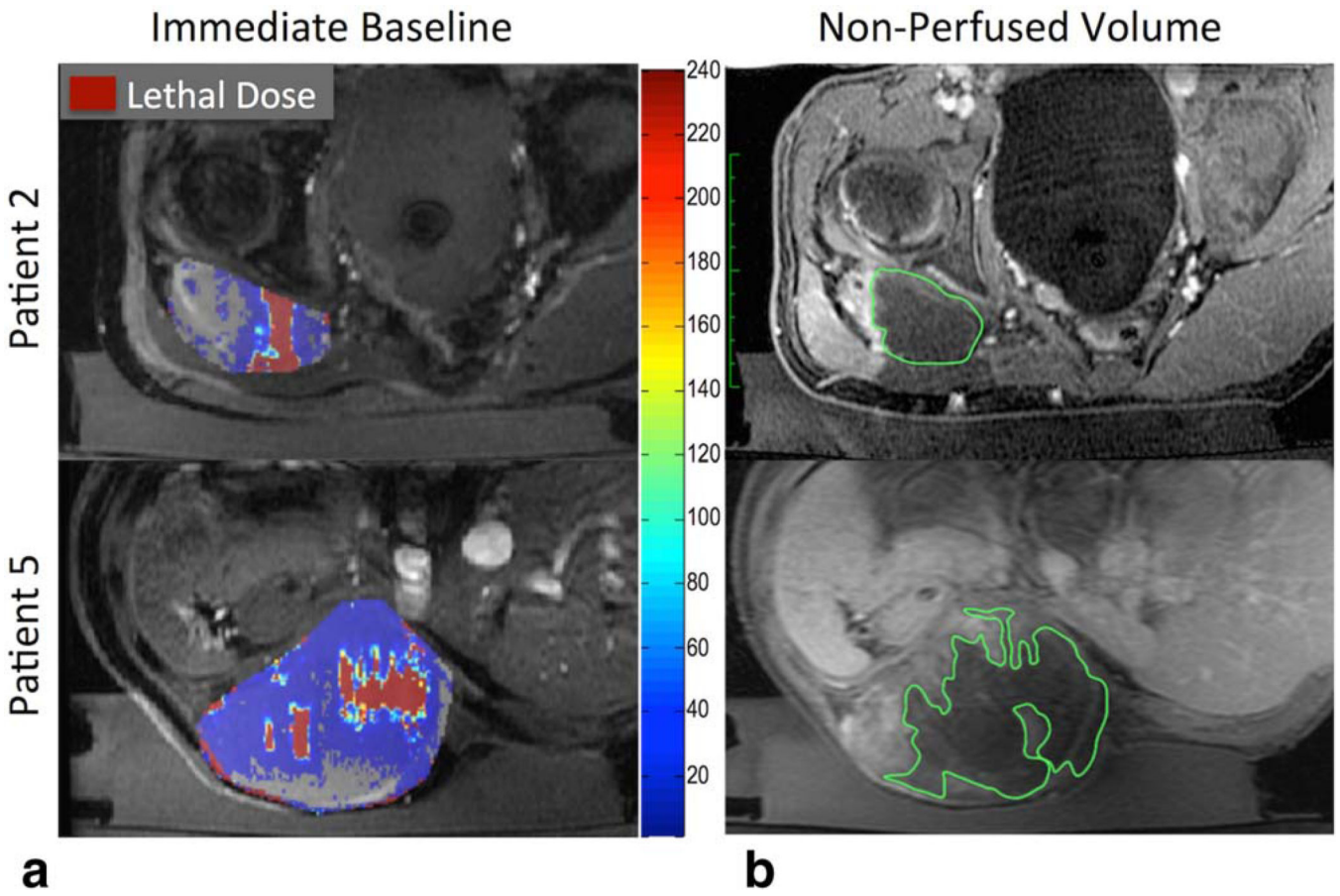

FIGURE 3.

Thermal dose overlay and contrast-enhanced images of a similar slice in two patients (rows). Column **(a)** shows immediate baseline calculated dose and **(b)** shows the NPV (green contour). Tumor region is outlined in gray. Lethal thermal dose is indicated by dark red pixels. Thermal dose (red) underestimates the amount of ablated tissue when compared to NPV (green).

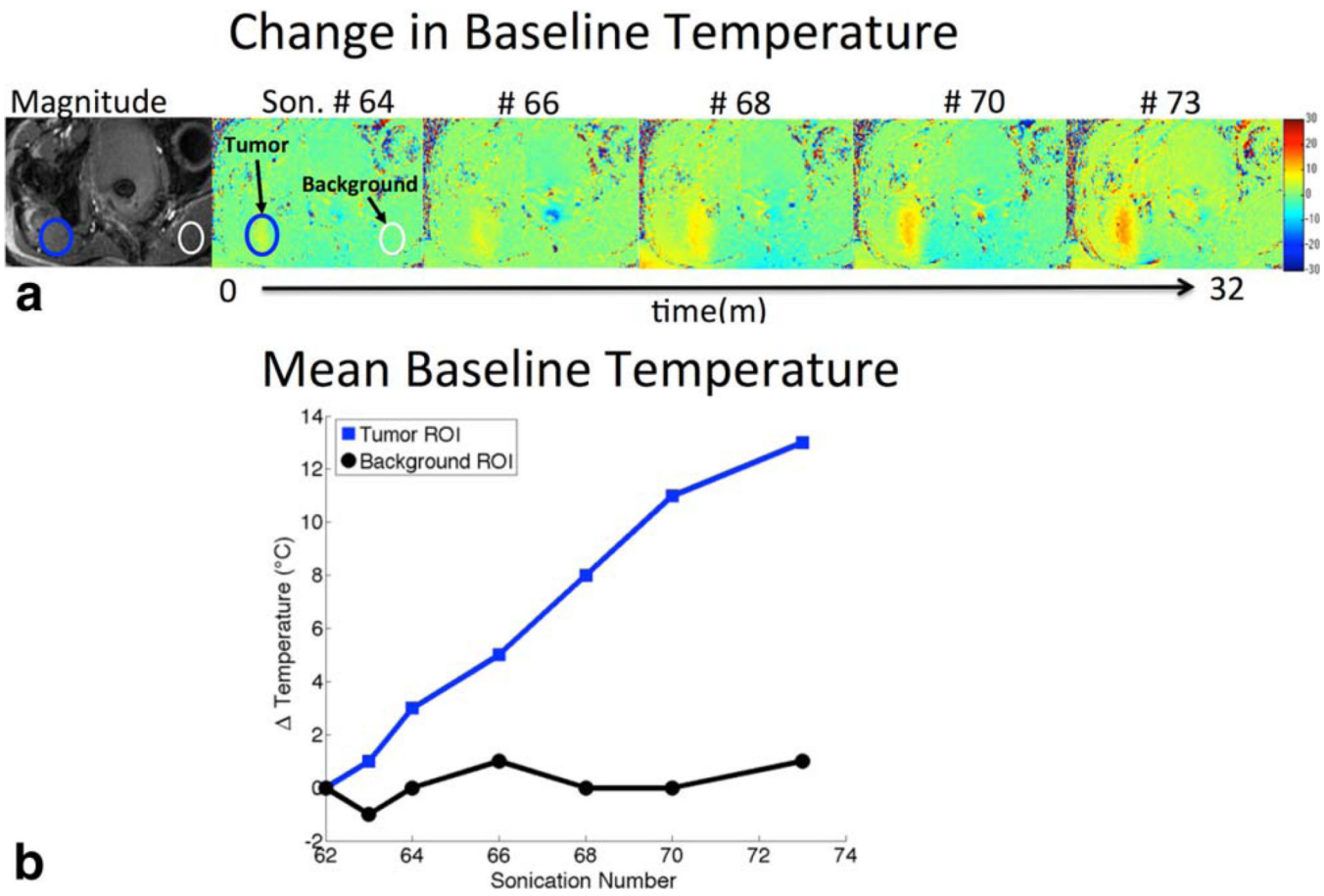

FIGURE 4.

a: Magnitude image of slice location (left). Baseline-to-baseline temperature maps of the same slice location over the course of a patient treatment. Sonication numbers indicated across the top, sonication #60 (not shown) was used as the reference for the subsequent baselines. **b:** Mean baseline temperatures of region of interests in the tumor, and background (where no heat is applied during the treatment), as a function of sonication number (indicating treatment time). Prior baseline processing shows subsequent preheating baselines in the treatment region do not actually return to body temperature where ΔT = 0°C, as assumed.

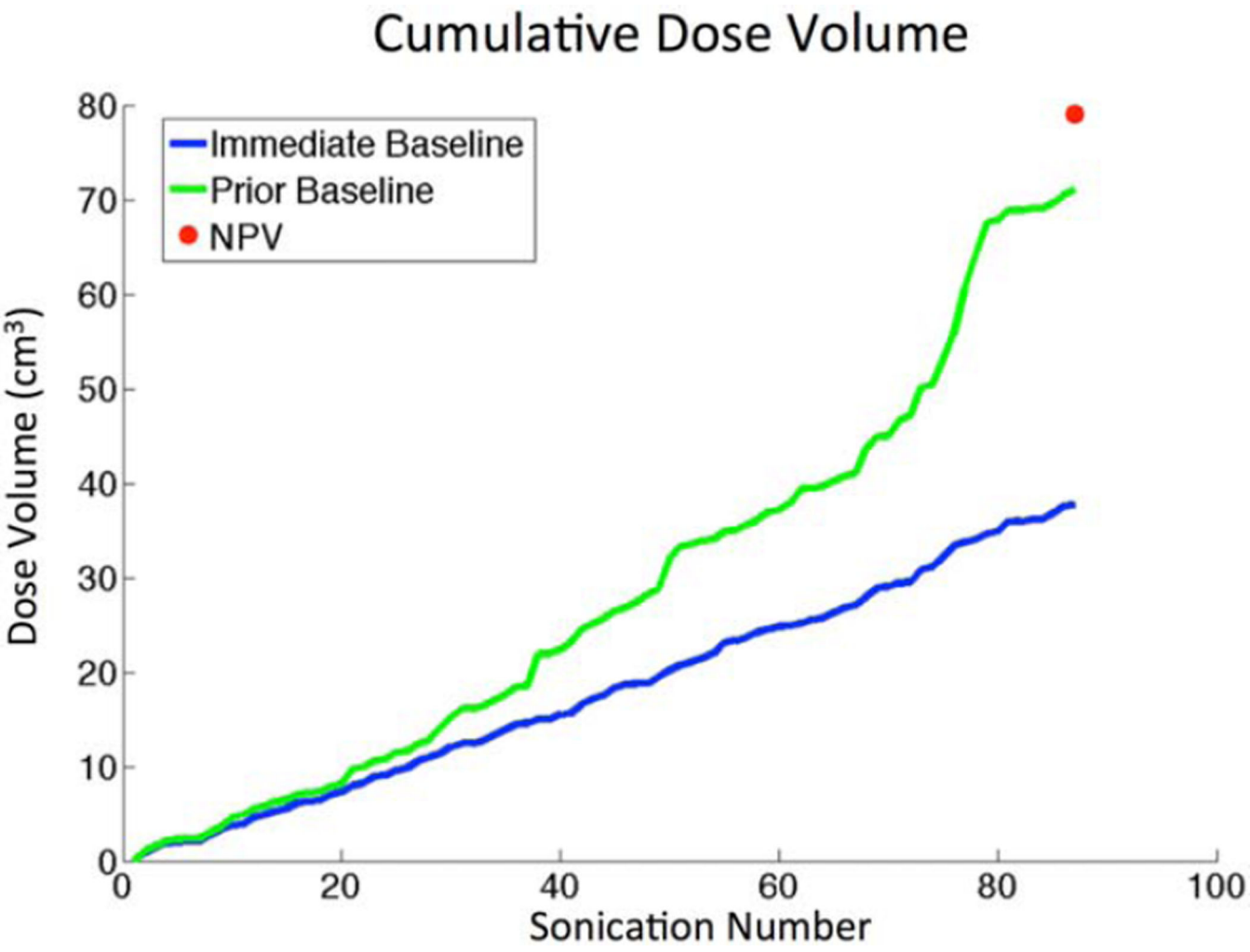

FIGURE 5.

Immediate vs. Prior Baseline comparison of cumulative dose volume over the long time course of a treatment for patient 2. Total treatment time was 3h:36m.

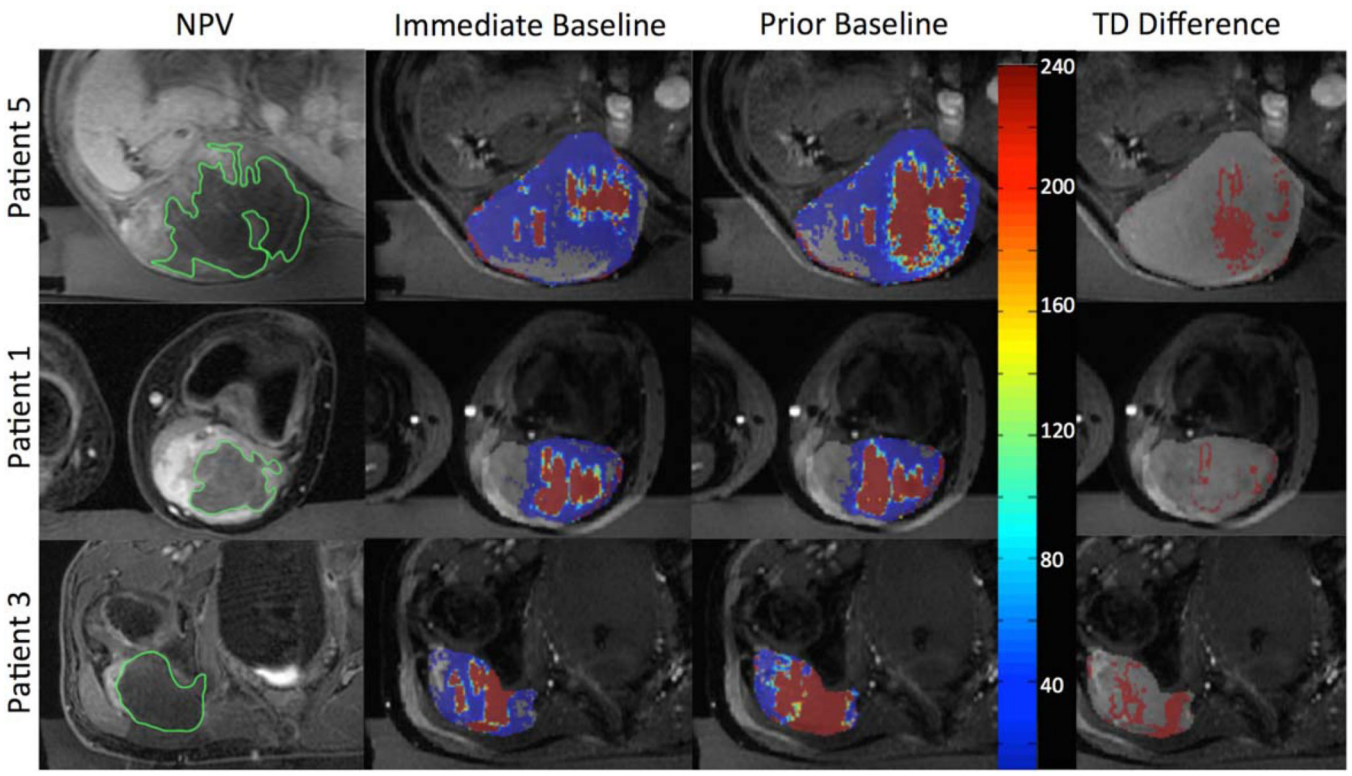

FIGURE 6.

Patient images showing **(a)** post treatment NPV (green), **(b)** immediate baseline (red), and **(c)** prior baseline treatment contours (red) for three patients. Column **(d)** is the additional dose calculated due to the prior baseline method. Gray overlay in columns (b–d) indicates general region of treatment.

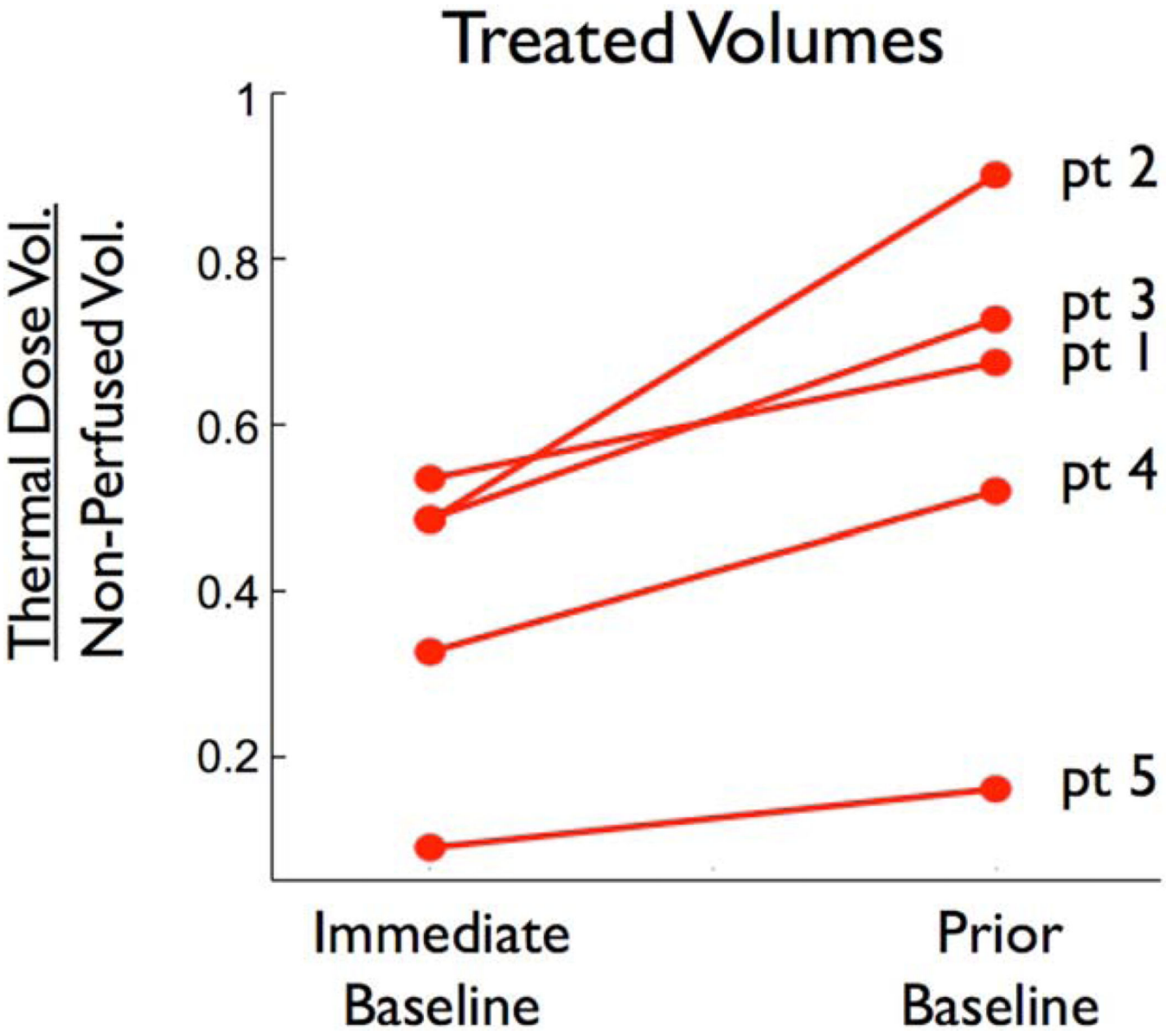

FIGURE 7.

Treatment volumes of all patients using immediate and prior baseline methods as a fraction of NPV. Patient numbers are listed on the right. A fraction of 1 indicates total agreement between thermal dose volume and NPV.

TABLE 1

Thermal Dose Treated Tumor Volume (TDV), Postcontrast Enhanced Nonperfused Treated Volume (NPV), and the Percent Error Between the Two Measures

	TDV (cc)	NPV (cc)	% Error
Patient 1	34	64	47%
Patient 2	38	79	52%
Patient 3	13	29	55%
Patient 4	20	62	68%
Patient 5	57	663	91%

TABLE 2

Performance of Prior Baseline Method for Each Patient

	Exist early baseline (%)	Used early baseline (%)	Mean baseline image no.
Patient 1	72	70	1.23
Patient 2	74	64	1.25
Patient 3	71	63	1.29
Patient 4	72	60	1.15
Patient 5	79	48	2.23

Columns indicate fraction of total sonications where a prior baseline existed, fraction of total sonications used in calculations (by meeting prior baseline matching criteria, where maximum value would be equal to exist early baseline), and the average baseline number used (where 1 indicates the earliest, or first baseline acquired, 2 is the second baseline, etc.). Most were able to utilize the earliest available baseline.